

Article

Highly Sensitive Electrochemical Aptasensor for Detecting the VEGF₁₆₅ Tumor Marker with PANI/CNT Nanocomposites

Yunjeong Park ^{1,†}, Min-Sung Hong ^{2,†}, Woo-Hyuk Lee ², Jung-Gu Kim ^{2,*} and Kyunghoon Kim ^{1,*} 

¹ School of Mechanical Engineering, Sungkyunkwan University (SKKU), Suwon 16419, Korea; djy828@skku.edu

² School of Advanced Materials Science and Engineering, Sungkyunkwan University (SKKU), Suwon 16419, Korea; smith803@skku.edu (M.-S.H.); picohiyo@skku.edu (W.-H.L.)

* Correspondence: kimjg@skku.edu (J.-G.K.); kenkim@skku.edu (K.K.)

† These authors contributed equally to this work.

Abstract: Sensing targeted tumor markers with high sensitivity provides vital information for the fast diagnosis and treatment of cancer patients. A vascular endothelial growth factor (VEGF₁₆₅) have recently emerged as a promising biomarker of tumor cells. The electrochemical aptasensor is a promising tool for detecting VEGF₁₆₅ because of its advantages such as a low cost and quantitative analysis. To produce a sensitive and stable sensor electrode, nanocomposites based on polyaniline (PANI) and carbon nanotube (CNT) have potential, as they provide for easy fabrication, simple synthesis, have a large surface area, and are suitable in biological environments. Here, a label-free electrochemical aptasensor based on nanocomposites of CNT and PANI was prepared for detecting VEGF₁₆₅ as a tumor marker. The nanocomposite was assembled with immobilized VEGF₁₆₅ aptamer as a highly sensitive VEGF₁₆₅ sensor. It exhibited stable and wide linear detection ranges from 0.5 pg/mL to 1 µg/mL, with a limit of detection of 0.4 pg/mL because of the complementary effect of PANI/CNT. The fabricated aptasensor also exhibited good stability in biological conditions, selectivity, and reproducibility after several measurement times after the dissociation process. Thus, it could be applied for the non-invasive determination of VEGF, in biological fluid diagnosis kits, or in an aptamer-based biosensor platform in the near future.

Keywords: aptasensor; aptamer; polyaniline (PANI); carbon nanotube (CNT); nanocomposite; electrochemical sensor; vascular endothelial growth factor (VEGF₁₆₅)



Citation: Park, Y.; Hong, M.-S.; Lee, W.-H.; Kim, J.-G.; Kim, K. Highly Sensitive Electrochemical Aptasensor for Detecting the VEGF₁₆₅ Tumor Marker with PANI/CNT Nanocomposites. *Biosensors* **2021**, *11*, 114. <https://doi.org/10.3390/bios11040114>

Received: 24 February 2021

Accepted: 6 April 2021

Published: 9 April 2021

Publisher's Note: MDPI stays neutral with regard to jurisdictional claims in published maps and institutional affiliations.



Copyright: © 2021 by the authors. Licensee MDPI, Basel, Switzerland. This article is an open access article distributed under the terms and conditions of the Creative Commons Attribution (CC BY) license (<https://creativecommons.org/licenses/by/4.0/>).

1. Introduction

Vascular endothelial growth factor (VEGF₁₆₅), a glycosylated protein belonging to the platelet-derived growth factor family of the cystine-knot growth factors, is essential for vascular development [1]. It is also active in angiogenesis, vasculogenesis, and endothelial cell growth, causing endothelial cell proliferation, promoting cell migration, inhibiting apoptosis, and inducing blood vessel permeabilization [2–4]. However, when tumor lymphatic vessels and metastasis of cancer are induced, abnormally fast growth and division of tumors can promote overexpression of VEGF₁₆₅ [5]. A high level of VEGF₁₆₅ can be regarded as a predictor of different cancers, such as brain, lung, breast, lymphoma, and gastrointestinal tumors [6–8]. Therefore, VEGF₁₆₅ has been recently suggested as a promising biomarker for diagnosing cancers [9–11]. In addition, VEGF-mediated eye disease is related to VEGF₁₆₅, and such patients have a VEGF concentration ranging from 74.5 to 521.6 pg/mL [12]. For the patient of VEGF drug treatment, there are a few significant studies on the detection of VEGF₁₆₅ levels in bio samples [13–16]; however, more accurate, reliable, and stable detection methods with higher sensitivity are still required.

Lately, aptamers have received attention in the field of biosensor due to their remarkable binding affinities and stability [17,18]. Aptamers contain an artificial oligo-nucleic acid or peptide molecule, which is a single-stranded DNA (ssDNA) or RNA [19]. Aptamers

are also called “chemical antibodies” due to their artificial process in vitro based on the systematic evolution of ligands by the exponential enrichment (SELEX) technique. Unlike the production of commercial antibodies, which depends on the derivation of an animal immune system, the SELEX process can synthesize aptamers for non-immunogenic and toxic targets [20]. For this reason, they can replace antibody bioassays because aptamers are easy to synthesize, highly resistant to denaturation, and low cost [21]. Due to their high specificity and affinity, which came from their ability of folding upon binding with their target molecule, aptamers can be selected in vitro for any given target, ranging from small molecules to large proteins and even cells, which can make various aptamer-based biosensors [22,23]. Biosensors made with aptamers based on various nanomaterials have been designed to detect very low concentrations of their targets [24–26]. However, it is still challenging to optimize the anchor of an aptamer on nanomaterials for aptamer-based biosensors (aptasensors).

Carbon nanotubes (CNTs) are among the most widely researched one-dimensional materials due to their excellent mechanical, heating, electrical, and optical properties [27]. Especially, CNTs are suitable for making electrode materials: because of their high electrical conductivities and diverse surface modification, CNTs provide an enhanced electrocatalytic reaction and good stability [28,29]. Because CNTs facilitate electron transfer between electroactive species and the electrode, they offer great promise for fabricating chemical sensors or biosensors [27,30]. Therefore, many studies have achieved high stability and electrical properties of CNTs by combining them with various effective materials. Not only that, but significant progress also has been made on nanocomposites with the synthesis of conductive polymer and CNTs, which show excellent potential to apply in various fields because of their outstanding physical and chemical characteristics originating from their small dimensions and high surface areas [31,32]. Among the conducting polymers, polyaniline (PANI) is a unique conjugated polymer that can be used for specific applications when it is combined with nanomaterials [33,34]. The incorporation of CNT with PANI acts as a network film that leads to a high carrier mobility and high surface-to-volume ratio; it also minimizes the loss of signal intensity because of the direct path for charge/ion transportation while offering improved sensitivity [35,36].

The objective of this study was to introduce a simple and highly sensitive electrochemical biosensor to detect VEGF₁₆₅ by incorporating PANI and CNT with an anti-VEGF₁₆₅ RNA aptamer on a screen-printed carbon electrode (SPCE). Such a biosensor can achieve a simple and accurate VEGF₁₆₅ detection as a powerful platform for bioanalysis and clinic diagnostic application. It can be used in various flexible devices due to the polymeric property of the PANI/CNT nanocomposite.

2. Materials and Methods

2.1. Materials

CNTs (purity > 95%, diameter ~1.5 nm, length = 1–5 μm) were commercially purchased from NanoLab (Waltham, MA, USA). H₂SO₄, HNO₃, ammonium persulfate (APS), aniline, and vascular endothelial growth factor (VEGF₁₆₅) were purchased from Sigma-Aldrich (St. Louis, MO, USA). Deionized (DI) water was used for PANI/CNT synthesis and washing purposes. SPCE was obtained from EG Tech (Bucheon, Korea). Anti-VEGF₁₆₅ RNA aptamer was obtained from Bioneer Co. (Daejeon, Korea). The aptamer sequence was as follows: 5'-NH₂-AUG CAG UUU GAG AAG UCG CGC AU-3'.

2.2. Fabrication of PANI/CNT Nanocomposite on SPCE

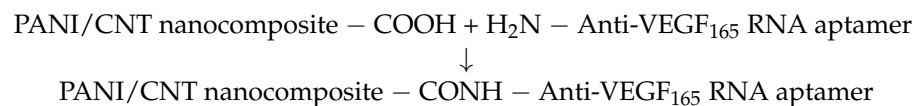
Carboxylic acid functionalized CNTs were prepared according to the conventional oxidation method [37]. Pristine CNTs (100 mg) were suspended in 24 mL mixture of concentrated H₂SO₄/HNO₃ (3:1, v/v). They were then sonicated in a water bath at 35–45 °C for 24 h. After cooling to room temperature, the suspension was then filtered with 200 nm porous filter membrane (PTFE; Millipore). Filtrated materials were washed several times

with DI water until a neutral pH was obtained. Collected materials were then dried in a vacuum oven at 50 °C for 12 h.

Functionalized CNTs were suspended in DI water and sonicated in a water bath at 25 °C for 30 min to prepare a 0.5 mg/mL CNT solution. A suspension (45 µL) of functionalized CNTs was added to 1 M HCl (6 mL) and sonicated in a water bath at 25 °C for 15 min. After adding 9 mg of APS, the mixture was sonicated for 15 min. The mixture was then placed in a refrigerator at 5 °C for 30 min. After 6.5 µL of aniline was dropped into the above mixture, the mixture was then dropped on the SPCE surface and dried overnight at 40 °C for further characterization. PANI-only nanocomposites were also prepared with the above method without adding CNTs.

2.3. Immobilization of Aptamer on PANI/CNT Nanocomposite

Aptamer stock solution was diluted with diethylpyrocarbonate (DEPC)-treated water (0.1 wt%) and stored at −20 °C in a freezer before use. To attach the anti-VEGF₁₆₅ RNA aptamer onto the surface of the PANI/CNT nanocomposite, a mixture of anti-VEGF₁₆₅ RNA aptamer (10 nM) and 4-(4,6-Dimethoxy-1,3,5-triazin-2-yl)-4-methyl-morpholinium chloride (DMT-MM) solution (1 wt%; 40 µL) was incubated with the SPCE surface for 12 h. DMT-MM is an efficient condensing agent. It was prepared according to the published description [38]. The condensing process on the surface can be expressed as follows [32]:



Afterwards, the SPCE was rinsed with DI water and dried with a stream of nitrogen gas (Figure 1).

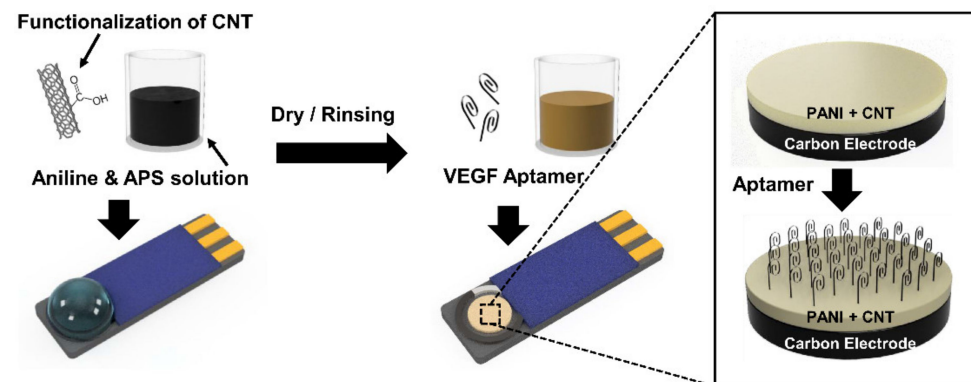


Figure 1. Schematic illustration of the preparation of the polyaniline/carbon nanotube (PANI/CNT) nanocomposite and the assembled VEGF₁₆₅ aptamer on the sensor surfaces for the VEGF sensors.

2.4. Characterization of the Biosensor

Surface morphology was observed using a scanning electron microscope (SEM; JSM-7600F, Jeol Ltd., Tokyo, Japan). For the surface elements analysis, Fourier-transform infrared (FT-IR) spectra of the PANI/CNT were obtained using an IFS-66/S FT-IR spectrometer (Bruker, Ettlingen, Germany) and an X-ray photoelectron spectroscope (XPS) recorded with ESCALAB250 equipment (Thermo Electron, Waltham, MA, USA) and an Al K α monochromatic X-ray source ($h\nu = 1486.6$ eV).

2.5. Electrochemical Analysis to Evaluate the Sensitivity of the Biosensor

For a three-electrode system of the SPCE, a working electrode (WE) and a counter electrode (CE) were printed with carbon ink. Silver (Ag) ink was used as the reference electrode (RE). The three-electrode system of SPCE was connected to an electrochemical apparatus (VSP 300, Bio-Logic SAS, Seyssinet-Pariset, France). All electrochemical tests

were performed in 10 mM $(\text{Fe}(\text{CN})_6)^{3-/4-}$ as the redox agent in a PBS buffer solution, resulting in a charge transfer resistance. Cyclic voltammetry (CV) tests were conducted at the voltage range of -0.2 V to 0.7 V with a scan rate of 50 mV/sec. Electrochemical impedance spectroscopy (EIS) was carried out with an amplitude of 20 mV in a frequency range of 100 kHz to 10 MHz. The potential was set to be 0.2 V (vs. Ag/AgCl) for all EIS measurements. Impedance plots were interpreted on the basis of equivalent circuits using a suitable fitting procedure with ZsimpWin software (ZsimpWin 3.20, EChem Software, Ann Arbor, MI, USA). Differential pulsed voltammetry (DPV) tests were performed at the voltage ranging from -0.2 V to 0.4 V with a pulse height of 50 mV and pulse width of 50 ms. Step height and step time of the DPV tests were set at 5 mV and 500 ms, respectively. The selectivity of the modified biosensor was compared using other bio-proteins, such as human serum albumin (HSA), human immunoglobulin (HIgG), lipase (Lip), and lysine (Lys), which were used as interference molecules.

3. Results and Discussion

3.1. Characterization of the PANI/CNT Nanocomposite

Acid-treated CNTs have high dispersity in an aqueous environment due to various functional groups such as hydroxyl and carboxyl groups. These functional groups can act as active sites that are capable of attaching some anilinium ions by electrostatic attraction. Thus, polymerization of aniline on the active sites of CNTs make the PANI/CNT nanocomposites. For comparison, SEM images of PANI (Figure 2A,B) and PANI/CNT (Figure 2C,D) were obtained to characterize their morphologies. The PANI-modified electrode showed porous nano-fibril structures [39,40]. On the other hand, the PANI/CNT-modified electrode showed individual fibers, indicating that the PANI covered the surface of the CNTs because the active sites of the CNTs could act as a backbone for PANI [36,39,40].

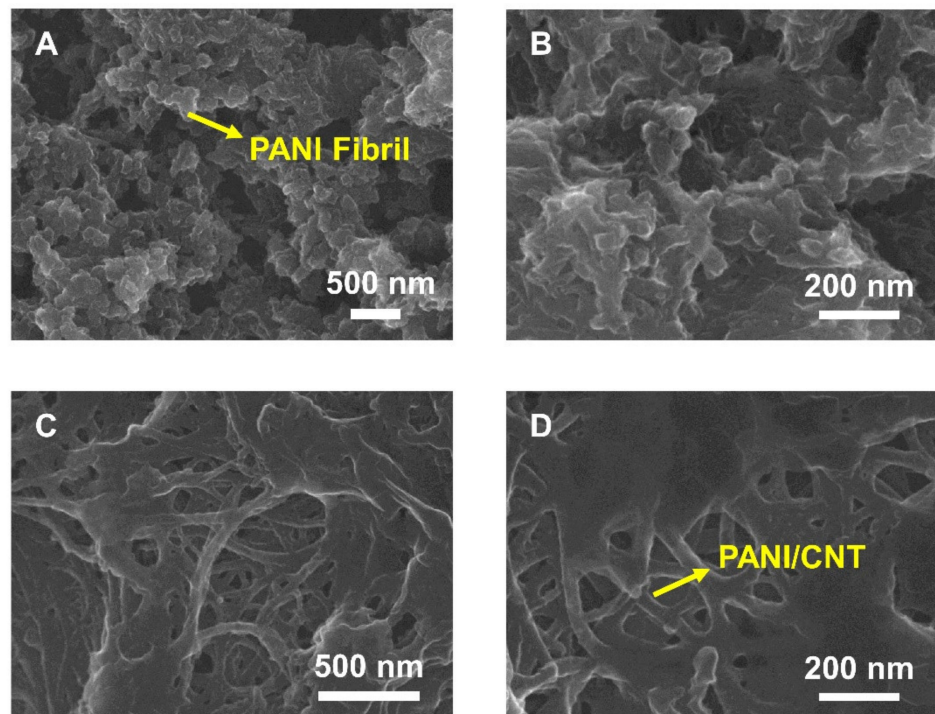


Figure 2. Scanning electron microscope (SEM) images of (A) PANI and (B) an enlarged image of PANI. (C) The PANI/CNT nanocomposite and (D) an enlarged image of the PANI/CNT nanocomposite.

FT-IR spectra were obtained to determine the chemical constitutions of the PANI/CNT nanocomposite. As shown in Figure 3, PANI had distinct peaks at 1550cm^{-1} , 1483cm^{-1} , and 1299cm^{-1} , representing the quinoid ring, benzenoid ring, and C–N stretching mode of the second arylamine, respectively, indicating an oxidation state of emeraldine salt (ES)

of PANI. In addition, a strong peak at around 1130 cm^{-1} , representing an electron-like band, was found for PANI [36]. CNT had large peaks at 3440 cm^{-1} , 1634 cm^{-1} , and 1100 cm^{-1} , representing O–H stretching from the carboxyl group (O=C–OH and C–OH), the stretching of C=C in the quinoid ring, and C–O stretching vibrations, respectively. The PANI/CNT nanocomposite showed obvious peaks at 1632 cm^{-1} and 1470 cm^{-1} , representing the quinoid ring of the C=C structure of the CNT and benzenoid ring of the ES state of the PANI chains, similar to the FT-IR spectra of the PANI/CNT. These results indicate that the surface of the CNTs was coated with PANI to successfully form the PANI/CNT nanocomposite.

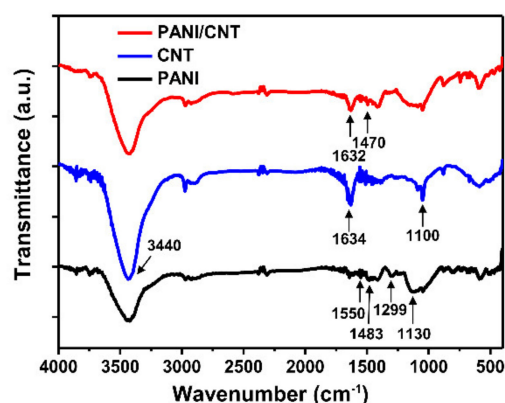


Figure 3. Fourier-transform infrared spectroscopy (FT-IR) spectra of the PANI, CNT, and PANI/CNT nanocomposites.

3.2. Characterization of Biosensor Based on SPCE

To characterize the modification of the SPCE electrode with the PANI/CNT and aptamer, deconvoluted XPS spectra of wide scan, C1s, N1s, and P2p were obtained, as shown in Figure 4. In the wide scan (Figure 4A), the N and O peaks were increased while the peaks of C decreased after aptamer immobilization due to the configuration of the aptamer with higher compositions of N and O but a lower composition of C. In addition, the P2p peak at 133 eV was found as a strong proof of successful immobilization of aptamers [41]. As shown in Figure 4B, the C1s spectrum had peaks similar to the PANI layer and PANI/CNT layer that appeared at 286.13 eV (–COOH group), 285.28 eV (sp^3C and C=N bond), and 284.48 eV (sp^2C and C–N bond). After the electrodes were modified with aptamers (PANI/CNT/Apt), the N–C=O peak corresponding to covalent bonding between the PANI/CNT and aptamer and C=O peak of the aptamer component newly appeared at 286.88 eV and 285.33 eV, respectively. In addition, the –COOH group peak shifted slightly to a higher energy at 288.15 eV. As shown in Figure 4C, N1s spectrum of PANI also had two peaks at 399.48 eV (–NH) and 401.38 eV (–NH and $-\text{N}^+$). When PANI was combined with CNT, it showed a peak at 402.88 eV ($-\text{N}^+$), indicating a higher binding energy. The PANI/CNT/Apt layer exhibited three new peaks at 400.68 eV (HNC=O), 399.18 eV (–NH), and 397.958 eV (C=N), indicating that a covalent bond was formed between the COOH group of the PANI/CNT and the NH_2 of aptamer [41]. Moreover, the P2p spectrum of the PANI/CNT showed no peak, while the PANI/CNT/Apt layer showed a phosphate peak at 132.73 eV due to the aptamer molecules (Figure 4D) [41]. These results demonstrated that the PANI/CNT/Apt nanocomposite was successfully synthesized.

3.3. Electrochemical Property of the Biosensor Based on an Aptamer with a PANI/CNT Nanocomposite

To elucidate the effect of the PANI/CNT film, the electrochemical properties of the composite film were evaluated with CV and EIS measurements in a test solution. According to the voltammogram results, which is shown in Figure 5A and Figure S2, the PANI, PANI/CNT, and PANI/CNT/Apt nanocomposite clearly had different electrochemical behaviors. After modification of the bare electrode with the PANI or PANI/CNT nanocom-

posite, the oxidation peak potential of the ferricyanide was increased due to its electrical conductivity. However, the PANI/CNT electrode had a higher conductivity than the PANI electrode because of the excellent electronic properties of the CNTs. The PANI/CNT nanocomposite clearly demonstrated stronger peaks, indicating that the nanocomposite had more electroactive sites than the PANI electrode. However, after the aptamer immobilization reaction, the redox peak of the PANI/CNT/Apt was dramatically decreased compared to that of PANI or PANI/CNT. This result indicates that the charge transfer resistance was increased because immobilization of the aptamers on electrode surface blocked the path of the redox reaction substance.

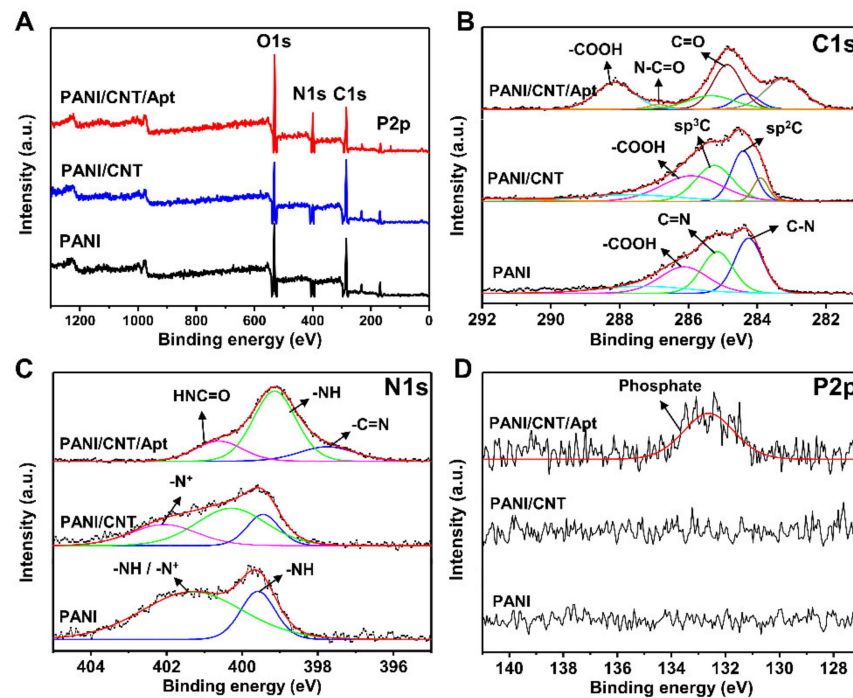


Figure 4. X-ray photoelectron spectroscopy (XPS) spectra of the modified electrode surfaces with PANI, PANI/CNT and PANI/CNT/Apt. (A) XPS wide spectra of the modified surfaces. (B) High-resolution XPS spectra of C1s, (C) N1s, and (D) P2p.

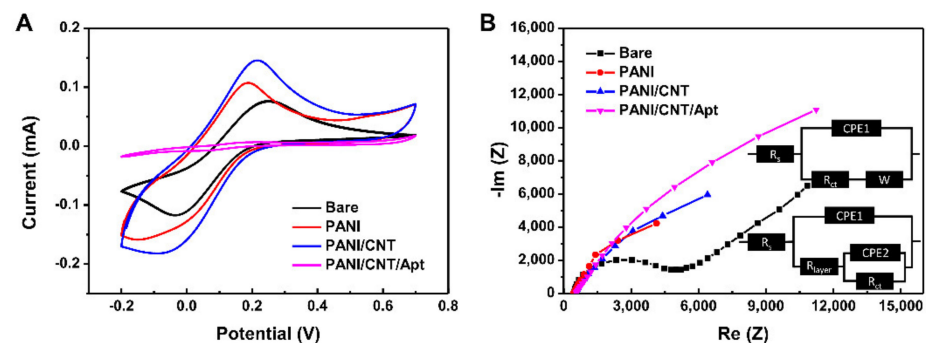


Figure 5. (A) Cyclic voltammetry (CV) at scan rate of 50 mV/sec and (B) the electrochemical impedance spectroscopy (EIS) at 0.2 V (vs. Ag/AgCl) in the frequency range of 100 kHz to 10 MHz spectra in 10 mM $(\text{Fe}(\text{CN})_6)^{3-/4-}$ as the redox PBS buffer solution measured on PANI, PANI/CNT, and PANI/CNT/Apt-modified electrodes and unmodified SPCE. The inset is the electric circuit compatible with the Nyquist diagrams for the modified electrodes. R_s : Electrolyte resistance; R_{ct} : Charge transfer resistance; CPE1: Constant phase element; and W: Warburg diffusion impedance.

Differences in the modified electrodes were also determined by EIS test. The results are shown in Figure 5B. In the EIS plots, the bare electrode shows the property of a

diffusion-limited process. On the other hand, the modified electrodes revealed semicircle curves, indicating that the electron transfer between $(\text{Fe}(\text{CN})_6)^{3-/4-}$ and the electrode was blocked by the PANI, PANI/CNT, and PANI/CNT/Apt layers on the electrode [16]. The circuits are described as two modes: electrolyte resistance (R_s), charge transfer resistance (R_{ct}), layer (coating) resistance (R_{layer}); CPE1 is the dielectric strength of the layer and solution absorbed by the layer and electric double layer at the electrolyte/substrate interface (CPE2) used for interface capacitance and Warburg diffusion impedance (W) at a low frequency [42,43]. In the EIS test results, the modified electrodes show incomplete semicircle features. There are two reasons for the incomplete semicircle: the frequency range of the EIS tests and their surface characteristics. The EIS results of the modified electrodes need a few more points at the low frequency region for a complete semicircle. However, it takes much more time to obtain the points in the low frequency region; therefore, generally, the frequency range is limited from 100 kHz to 10 MHz in the EIS test. For this reason, the EIS tests are used a simulation programs to obtain the calculated values from the tests. As shown in Figure S1, comparison of the R_{ct} values could indicate resistance of the specimen's surface. The R_{ct} of the PANI-coated electrode of SPCE was recorded to be 14,240 Ω . The addition of CNT to PANI resulted in a reduction of R_{ct} to be 9851 Ω , which is due to the high electrical conductivity of the CNT. After immobilization of aptamers, the R_{ct} was dramatically increased to 46,170 Ω because the aptamer blocks the active sites on the nanocomposite surface for charge transfer. In addition, electrostatic repulsion between the negatively charged aptamer and solution-phase $(\text{Fe}(\text{CN})_6)^{3-/4-}$ redox agent leads to suppressing the chemical reaction on the electrode surface [15]. As a result, in CV and EIS characterization, the Faraday currents and charge transfer resistance changes were consistent.

3.4. VEGF₁₆₅ Detection and Monitoring

Under an optimized experimental condition (described in the experimental section), analytical calibration was performed using the DPV test. Results are presented in Figure 6. As shown in Figure 6A, after incubating the PANI aptasensor, an enhanced peak current (I_{peak}) was observed with decreasing concentration of VEGF₁₆₅ due to the mass transfer limiting of $(\text{Fe}(\text{CN})_6)^{3-/4-}$ to the electrode surface by binding with VEGF₁₆₅ molecules. There was a linear relationship between I_{peak} and the logarithm of the VEGF₁₆₅ concentration (C_{VEGF}) in the range from 10 fg/mL to 1 $\mu\text{g/mL}$ ($I_{\text{peak}} = 2.776 + 1.951 \log C_{\text{VEGF}}$ ($R^2 = 0.968$), R = correlation coefficient), with a limit of detection (LOD) of 0.7 ng/mL ($3\sigma/S$).

For comparison, the sensing performance of the modified electrode with PANI/CNT is shown in Figure 6B. The PANI/CNT aptasensor showed significantly decreased response currents, with a linear regression equation of $I_{\text{peak}} = 5.505 + 2.25 \log C_{\text{VEGF}}$ ($R^2 = 0.977$). It showed an excellent sensitivity with an LOD of 0.4 pg/mL ($3\sigma/S$) because the electrode modified with PANI/CNT had a large specific area and electron transfer rate favorable for signal transmission. In addition, the peak current of the bare PANI/CNT electrode is higher than that of the PANI electrode due to the same reasons. These results confirmed that the PANI/CNT-modified electrode could enhance the electrochemical signal and contribute to the high performance in VEGF₁₆₅ detection. Besides, the PANI/CNT aptasensor showed comparable or better performance than other reported VEGF₁₆₅ biosensors (Table 1). Considering the design of a diverse aptamer for a biosensor and the simple preparation process of the PANI/CNT-modified electrode, the high-performance of the PANI/CNT aptasensor fabricated in this study would have wide bio-applications.

3.5. Selectivity

Selectivity results of the PANI/CNT/Apt nanocomposite in sensing response to VEGF₁₆₅ compared to other bio-proteins at the certain concentrations are shown in Figure 7. To evaluate the selectivity of the proposed aptasensor, some biomolecules, such as HSA, HlgG, Lip, and Lys, were used as interference molecules, which is the major nonspecific binding constituents of human serum blood. This process was performed to evaluate the

selectivity to VEGF₁₆₅ of the PANI/CNT/Apt aptasensor within the interfering agents. The base concentration of the VEGF₁₆₅ was selected as 100 pg/mL and 10 ng/mL, and the concentration of the interference proteins was applied to 100 times higher than the base VEGF₁₆₅ concentrations. As clearly shown in Figure 7, the results showed a negligible effect on the main signal. For example, HIgG resulted in only about a 0.5% error in the detection of VEGF₁₆₅. This was because the physical adsorption of HIgG onto the surface-modified electrode can be easily washed away by the PBS rinsing. As expected, the proposed aptasensor possessed a high sensitivity for VEGF₁₆₅ due to a high affinity and specificity of the aptasensor toward the presence of specific nucleic acid sequences in their structures that could bind a specific target.

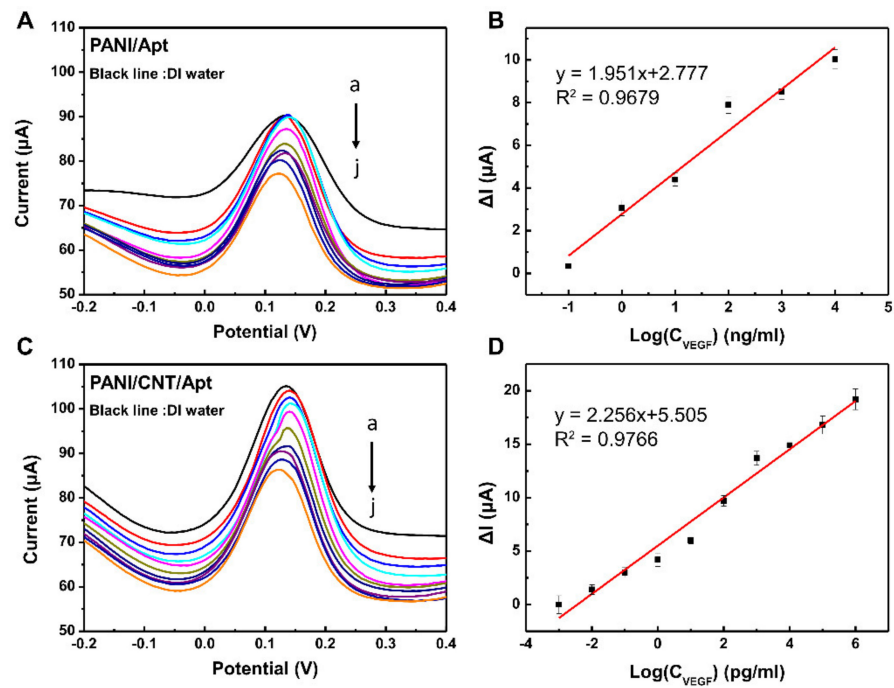


Figure 6. (A,C) Differential pulse voltammetry (DPV) plot, at range from -0.2 V to 0.4 V with a 5 mV height and 50 ms pulse width (step height: 5 mV and step time: 500 ms), of VEGF₁₆₅ at different concentrations (from a to j): (reference black line: DI water) 10 fg/mL, 100 fg/mL, 1 pg/mL, 10 pg/mL, 100 pg/mL, 1 ng/mL, 10 ng/mL, 100 ng/mL, 1 μ g/mL, and 10 μ g/mL under the optimized conditions on the PANI/Apt- and PANI/CNT/Apt-modified electrodes. (B,D) Peak currents vs. log VEGF concentrations from the DPV plots.

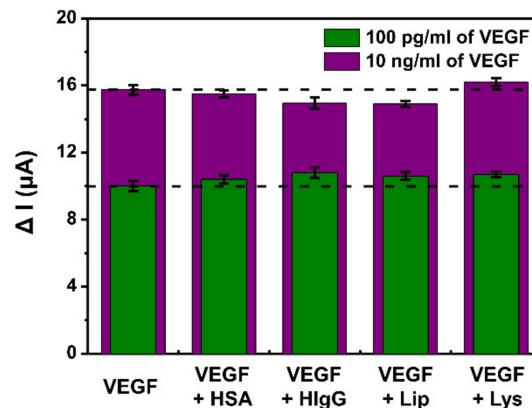


Figure 7. Selectivity of the PANI/CNT/Apt-modified electrodes shown in ΔI scales for VEGF₁₆₅ in the presence of 100 times of HSA, HIgG, Lip, and Lys as the interfering species. The concentrations of VEGF₁₆₅ are 100 pg/mL and 10 ng/mL and the interfering species are 10 ng/mL and 1 μ g/mL.

Table 1. Comparison of the VEGF sensor based on the nanomaterial-modified electrodes.

Modified Electrode	Detection Method	Linear Range (pg/mL)	LOD (pg/mL)	Reference
GE/GO/ssDNA/PLLA NP	DPV	50.0–1.0 × 10 ⁵	50	Pan et al. 2017 [11]
PPy-NDFLG-FETs/Apt	FET	4.5–4.5 × 10 ⁵	4.5	Kwon et al. 2012 [13]
GE/Apt/MB-Abs	nFIS	5.0–1.0 × 10 ³	401.0	Qureshi et al. 2015 [14]
SPE/OMC-Au _{nano} /Apt	EIS	10.0–300.0	1.0	Tabrizi et al. 2015 [15]
GE/Thiolated Apt	SWV	150.0–1.0 × 10 ⁵	150.0	Crulhas et al. 2017 [17]
CPNT-FETs/Apt	FET	18.0–18.0 × 10 ⁷	18.0	Kwon et al. 2010 [32]
SiNW-FETs/Apt	FET	100.0–45.0 × 10 ³	100.0	Lee et al. 2009 [44]
SPE/PANI/CNT/Apt	DPV	0.5–10.0 × 10 ⁶	0.4	This work

(GE: Gold-based screen-printed electrode; GO: Graphene oxide; PLLA NP: Poly-L-lactide nanoparticle; PPy-NDFLG: Polypyrrole-converted nitrogen-doped few-layer graphene; FET: Field effect transistor; Apt: Aptamer; MB-Abs: Antibody conjugated magnetic beads; nFIS: Non-Faradaic electrochemical impedance spectroscopy; SPE: Carbon-based screen-printed electrode; OMC-Aunano: Ordered mesoporous carbon-gold nanocomposite; SWV: Square wave voltammetry CPNTs: carboxylated polypyrrole nanotubes; SiNW: Silicon nanowire).

Intra- and inter-reproducibility of the proposed aptasensor were also considered. The same as with the selectivity tests, the electrodes were rinsed in a PBS solution. The intra reproducibility was estimated by measuring 100 pg/mL of VEGF₁₆₅ with the same aptasensor. The relative standard deviation (RSD) for a series of five experiments was found to be 5.6%. The inter reproducibility was evaluated with five difference aptasensors for determining 100 pg/mL of VEGF₁₆₅. The RSD was calculated to be 6.8%. These results showed that the proposed aptasensor exhibited high analytical performance in terms of sensitivity, selectivity, reproducibility, stability, and low detection limit.

4. Conclusions

In conclusion, we successfully fabricated a highly sensitive VEGF₁₆₅ detection sensor for cancer diagnosis. The sensor was assembled from a PANI/CNT nanocomposite by polymerization of APS and aniline at the CNT edge site with simultaneous film deposition. It exhibited high sensitivity for VEGF₁₆₅ sensing with an excellent detection limit of 0.4 pg/mL (3σ/S) compared to other reported biosensors. It also showed highly selectivity in the presence of other proteins. Such an excellent sensing performance was ascribed to the complementary effects of the PANI/CNT surface area, effective network channels of the PANI/CNT, and the highly selective reaction of the aptamer. The film has the advantages of a simple preparation, high sensitivity, small size, and the possibility of modification by changing the aptamer for sensing other bio-molecules. Thus, it has potential for use in highly effective and sensitive bio-sensor devices in the future.

Supplementary Materials: The following are available online at <https://www.mdpi.com/article/10.3390/bios11040114/s1>, Figure S1: Comparison of the electron charge transfer resistance on the bare and modified electrodes; Figure S2: The cyclic voltammetry spectra in redox buffer solution measured on PANI/CNT/Apt-modified electrode (Zoomed graph of Figure 5A.).

Author Contributions: Conceptualization, Y.P, M.-S.H., J.-G.K. and K.K.; methodology, Y.P.; software, M.-S.H.; validation, Y.P, M.-S.H. and K.K.; formal analysis, M.-S.H.; investigation, Y.P. and M.-S.H.; data curation, W.-H.L.; writing—original draft preparation, Y.P. and M.-S.H.; writing—review and editing, J.-G.K. and K.K.; visualization, Y.P. and M.-S.H.; supervision, J.-G.K. and K.K.; project administration, J.-G.K. and K.K.; funding acquisition, Y.P, M.-S.H., J.-G.K. and K.K. All authors have read and agreed to the published version of the manuscript.

Funding: This research was funded by the National Research Foundation of Korea (NRF) grant funded by the Korea government (NRF-2020R1A2C4002557 and NRF-2019M3A9H1103737). This work was also supported by grants (NRF-2018H1A2A1062418 and NRF-2020R1I1A1A01074866) of NRF funded by the Korean Government (NRF-2018-Fostering Core Leaders of the Future Basic Science Program/Global Ph.D. Fellowship Program and NRF-2020-Research Staff Program).

Institutional Review Board Statement: Not applicable.

Informed Consent Statement: Not applicable.

Data Availability Statement: Not applicable.

Conflicts of Interest: The authors declare no conflict of interest.

References

1. Michael, K.; Patricia, A.D. Vascular endothelial growth factor and its receptors. *Cytokine Growth Factor Rev.* **1996**, *7*, 259–270. [[CrossRef](#)]
2. Apte, R.S.; Chen, D.S.; Ferrara, N. VEGF in signaling and disease: Beyond discovery and development. *Cell* **2019**, *176*, 1248–1264. [[CrossRef](#)]
3. Bamburowicz-Klimkowska, M.; Poplawska, M.; Grudzinski, I.P. Nanocomposites as biomolecules delivery agents in nanomedicine. *J. Nanobiotechnol.* **2019**, *17*, 48. [[CrossRef](#)] [[PubMed](#)]
4. Simons, M.; Gordon, E.; Claesson-Welsh, L. Mechanisms and regulation of endothelial VEGF receptor signalling. *Nat. Rev. Mol. Cell Biol.* **2016**, *17*, 611–625. [[CrossRef](#)] [[PubMed](#)]
5. Loureiro, R.M.B.; D’Amore, P.A. Transcriptional regulation of vascular endothelial growth factor in cancer. *Cytokine Growth Factor Rev.* **2005**, *16*, 77–89. [[CrossRef](#)] [[PubMed](#)]
6. Ferrara, N.; Gerber, H.-P.; LeCouter, J. The biology of VEGF and its receptors. *Nat. Med.* **2003**, *9*, 669–676. [[CrossRef](#)]
7. Brattström, D.; Bergqvist, M.; Hesselius, P.; Larsson, A.; Wagenius, G.; Brodin, O. Serum VEGF and bFGF adds prognostic information in patients with normal platelet counts when sampled before, during and after treatment for locally advanced non-small cell lung cancer. *Lung Cancer* **2004**, *43*, 55–62. [[CrossRef](#)]
8. Ferrara, N. Vascular endothelial growth factor: Basic science and clinical progress. *Endocr. Rev.* **2004**, *25*, 581–611. [[CrossRef](#)]
9. Carenza, E.; Jordan, O.; Segundo, P.M.-S.; Jirik, R.; Starcuk, Z.; Borchard, G.; Rosell, A.; Roig, A. Encapsulation of VEGF₁₆₅ into magnetic PLGA nanocapsules for potential local delivery and bioactivity in human brain endothelial cells. *J. Mater. Chem. B* **2015**, *3*, 2538–2544. [[CrossRef](#)]
10. Kim, Y.; Jeong, S.; Jung, K.O.; Song, M.G.; Lee, C.-H.; Chung, S.; Park, J.Y.; Cha, M.G.; Lee, S.G.; Jun, B.-H.; et al. Simultaneous detection of EGFR and VEGF in colorectal cancer using fluorescence-raman endoscopy. *Sci. Rep.* **2017**, *7*, 1035. [[CrossRef](#)]
11. Pan, L.-H.; Kuo, S.-H.; Lin, T.-Y.; Lin, C.-W.; Fang, P.-Y.; Yang, H.-W. An electrochemical biosensor to simultaneously detect VEGF and PSA for early prostate cancer diagnosis based on graphene oxide/ssDNA/PLLA nanoparticles. *Biosens. Bioelectron.* **2017**, *89*, 598–605. [[CrossRef](#)]
12. Kim, M.; Lezzi, R.; Shim, B.S.; Martin, D.C. Impedimetric biosensors for detecting vascular endothelial growth factor (VEGF) based on poly (3,4-ethylene dioxythiophene) (PEDOT)/gold nanoparticle (AuNP) composites. *Front. Chem.* **2019**, *7*, 234. [[CrossRef](#)] [[PubMed](#)]
13. Kwon, O.S.; Park, S.J.; Hong, J.-Y.; Han, A.-R.; Lee, J.S.; Lee, J.S.; Oh, J.H.; Jang, J. Flexible FET-type VEGF aptasensor based on nitrogen-doped graphene converted from conducting polymer. *ACS Nano* **2012**, *6*, 1486–1493. [[CrossRef](#)] [[PubMed](#)]
14. Qureshi, A.; Gurbuz, Y.; Niazi, J.H. Capacitive aptamer–antibody based sandwich assay for the detection of VEGF cancer biomarker in serum. *Sens. Actuators B Chem.* **2015**, *209*, 645–651. [[CrossRef](#)]
15. Tabrizi, M.A.; Shamsipur, M.; Farzin, L. A high sensitive electrochemical aptasensor for the determination of VEGF₁₆₅ in serum of lung cancer patient. *Biosens. Bioelectron.* **2015**, *74*, 764–769. [[CrossRef](#)] [[PubMed](#)]
16. Shin, S.R.; Zhang, Y.S.; Kim, D.-J.; Manbohi, A.; Avci, H.; Silvestri, A.; Aleman, J.; Hu, N.; Kilic, T.; Keung, W.; et al. Aptamer-based microfluidic electrochemical biosensor for monitoring cell-secreted trace cardiac biomarkers. *Anal. Chem.* **2016**, *88*, 10019–10027. [[CrossRef](#)]
17. Crulhas, B.P.; Karpik, A.E.; Delella, F.K.; Castro, G.R.; Pedrosa, V.A. Electrochemical aptamer-based biosensor developed to monitor PSA and VEGF released by prostate cancer cells. *Anal. Bioanal. Chem.* **2017**, *409*, 6771–6780. [[CrossRef](#)]
18. Mehlhorn, A.; Rahimi, P.; Joseph, Y. Aptamer-based biosensors for antibiotic detection: A review. *Biosensors* **2018**, *8*, 54. [[CrossRef](#)]
19. Eissa, S.; Siaj, M.; Zourob, M. Aptamer-based competitive electrochemical biosensor for brevetoxin-2. *Biosens. Bioelectron.* **2015**, *69*, 148–154. [[CrossRef](#)]
20. Song, S.; Wang, L.; Li, J.; Fan, C.; Zhao, J. Aptamer-based biosensors. *Trac. Trends Anal. Chem.* **2008**, *27*, 108–117. [[CrossRef](#)]
21. Dunn, M.R.; Jimenez, R.M.; Chaput, J.C. Analysis of aptamer discovery and technology. *Nat. Rev. Chem.* **2017**, *1*, 0076. [[CrossRef](#)]
22. Hong, L.; Zhou, F.; Shi, D.; Zhang, X.; Wang, G. Portable aptamer biosensor of platelet-derived growth factor-BB using a personal glucose meter with triply amplified. *Biosens. Bioelectron.* **2017**, *95*, 152–159. [[CrossRef](#)] [[PubMed](#)]
23. Bala, R.; Kumar, M.; Bansal, K.; Sharma, R.K.; Wangoo, N. Ultrasensitive aptamer biosensor for malathion detection based on cationic polymer and gold nanoparticles. *Biosens. Bioelectron.* **2016**, *85*, 445–459. [[CrossRef](#)] [[PubMed](#)]
24. Forouzanfar, S.; Alam, F.; Pala, N.; Wang, C. A review of electrochemical aptasensors for label-free cancer diagnosis. *J. Electrochem. Soc.* **2020**, *167*, 067511. [[CrossRef](#)]
25. Yang, Y.; Yang, X.; Yang, Y.; Yuan, Q. Aptamer-functionalized carbon nanomaterials electrochemical sensors for detecting cancer relevant biomolecules. *Carbon* **2018**, *129*, 380–395. [[CrossRef](#)]
26. Mao, K.; Zhang, H.; Wang, Z.; Cao, H.; Zhang, K.; Li, X.; Yang, Z. Nanomaterial-based aptamer sensors for arsenic detection. *Biosens. Bioelectron.* **2020**, *148*, 111785. [[CrossRef](#)] [[PubMed](#)]

27. Schroeder, V.; Savagatrup, S.; He, M.; Lin, S.; Swager, T.M. Carbon nanotube chemical sensors. *Chem. Rev.* **2019**, *119*, 599–663. [[CrossRef](#)]
28. Cheng, J.; Wang, X.; Nie, T.; Yin, L.; Wang, S.; Zhao, Y.; Wu, H.; Mei, H. A novel electrochemical sensing platform for detection of dopamine based on gold nanobipyramid/multi-walled carbon nanotube hybrids. *Anal. Bioanal. Chem.* **2020**, *412*, 2433–2441. [[CrossRef](#)]
29. Landry, M.P.; Ando, H.; Chen, A.Y.; Cao, J.; Kottadiel, V.I.; Chio, L.; Yang, D.; Dong, J.; Lu, T.K.; Strano, M.S. Single-molecule detection of protein efflux from microorganisms using fluorescent single-walled carbon nanotube sensor arrays. *Nat. Nanotechnol.* **2017**, *12*, 368–377. [[CrossRef](#)]
30. Jones, L.P.; Stefansson, S.; Kim, M.S.; Ahn, S.N. Comparison of radioimmuno and carbon nanotube field-effect transistor assays for measuring insulin-like growth factor-1 in a preclinical model of human breast cancer. *J. Nanobiotechnol.* **2011**, *9*, 36. [[CrossRef](#)] [[PubMed](#)]
31. Yoon, H.; Jang, J. Conducting-polymer nanomaterials for high-performance sensor applications: Issues and challenges. *Adv. Funct. Mater.* **2009**, *19*, 1567–1576. [[CrossRef](#)]
32. Kwon, O.S.; Park, S.J.; Jang, J. A high-performance VEGF aptamer functionalized polypyrrole nanotube biosensor. *Biomaterials* **2010**, *31*, 4740–4747. [[CrossRef](#)]
33. Keteklahijani, Y.Z.; Sharif, F.; Roberts, E.P.L.; Sundararaj, U. Enhanced sensitivity of dopamine biosensors: An electrochemical approach based on nanocomposite electrodes comprising polyaniline, nitrogen-doped graphene, and DNA-functionalized carbon nanotubes. *J. Electrochem. Soc.* **2019**, *166*, 1415–1425. [[CrossRef](#)]
34. Sen, T.; Mishra, S.; Shimpi, N.G. Synthesis and sensing applications of polyaniline nanocomposites: A review. *RSC Adv.* **2016**, *6*, 42196–42222. [[CrossRef](#)]
35. Wan, P.; Wen, X.; Sun, C.; Chandran, B.K.; Zhang, H.; Sun, X.; Chen, X. Flexible transparent films based on nanocomposite networks of polyaniline and carbon nanotubes for high-performance gas sensing. *Small* **2015**, *11*, 5409–5415. [[CrossRef](#)] [[PubMed](#)]
36. Xue, L.; Wang, W.; Guo, Y.; Liu, G.; Wan, P. Flexible polyaniline/carbon nanotube nanocomposite film-based electronic gas sensors. *Sens. Actuators B Chem.* **2017**, *244*, 47–53. [[CrossRef](#)]
37. Hong, M.-S.; Park, Y.; Kim, T.; Kim, K.; Kim, J.-G. Polydopamine/carbon nanotube nanocomposite coating for corrosion resistance. *J. Materiomics.* **2020**, *6*, 158–166. [[CrossRef](#)]
38. Kunishima, M.; Kawachi, C.; Hioki, K.; Terao, K.; Tani, S. Formation of carboxamides by direct condensation of carboxylic acids and amines in alcohols using a new alcohol- and water-soluble condensing agent: DMT-MM. *Tetrahedron* **2001**, *57*, 1551–1558. [[CrossRef](#)]
39. Kaykha, Y.; Rafizadeh, M. Template synthesis of fibrillar polyaniline complex using a degradable polyelectrolyte. *Mater. Chem. Phys.* **2019**, *229*, 98–105. [[CrossRef](#)]
40. Maity, D.; Manoharan, M.; Kumar, R.T.R. Development of the PANI/MWCNT Nanocomposite-Based Fluorescent Sensor for Selective Detection of Aqueous Ammonia. *ACS Omega* **2020**, *5*, 8414–8422. [[CrossRef](#)]
41. Chung, S.; Moon, J.-M.; Choi, J.; Hwang, H.; Shim, Y.-B. Magnetic force assisted electrochemical sensor for the detection of thrombin with aptamer-antibody sandwich formation. *Biosens. Bioelectron.* **2018**, *117*, 480–486. [[CrossRef](#)] [[PubMed](#)]
42. Randviir, E.P.; Banks, C.E. Electrochemical impedance spectroscopy: An overview of bioanalytical applications. *Anal. Methods* **2013**, *5*, 1098–1115. [[CrossRef](#)]
43. Hong, M.-S.; Park, Y.; Kim, J.G.; Kim, K. Effect of incorporating MoS₂ in organic coatings on the corrosion resistance of 316L stainless steel in a 3.5% NaCl solution. *Coatings* **2019**, *9*, 45. [[CrossRef](#)]
44. Lee, H.-S.; Kim, K.S.; Kim, C.-J.; Hahn, S.K.; Jo, M.-H. Electrical detection of VEGFs for cancer diagnoses using anti-vascular endothelial growth factor aptamer-modified Si nanowire FETs. *Biosens. Bioelectron.* **2009**, *24*, 1801–1805. [[CrossRef](#)]